Steel and Composite Structures, *Vol. 38, No. 4 (2021) 431-445*
DOI: https://doi.org/10.12989/scs.2021.38.4.431

Shear behavior of concrete-encased square concrete-filled steel tube members: Experiments and strength prediction

Yong Yang[1,2], Xin Chen*[1], Yicong Xue[1], Yunlong Yu[1,2] and Chaorui Zhang[1]

[1]School of Civil Engineering, Xi'an University of Architecture and Technology, Xi'an, Shaanxi 710055, P.R. China
[2] Key Lab of Structural Engineering and Earthquake Resistance of the Ministry of Education, Xi'an University of Architecture and Technology, Xi'an, Shaanxi, P.R. China

(*Received October 3, 2020, Revised February 10, 2021, Accepted February 11, 2021*)

Abstract. This paper presents experiments and theoretical analysis on shear behavior of eight concrete-encased square concrete-filled steel tube (CECFST) specimens and three traditional reinforced concrete (RC) specimens. A total of 11 specimens with the test parameters including the shear span-to-depth ratio, steel tube size and studs arrangement were tested to explore the shear performance of CECFST specimens. The failure mode, shear capacity and displacement ductility were thoroughly evaluated. The test results indicated that all the test specimens failed in shear, and the CECFST specimens enhanced by the interior CFST core exhibited higher shear capacity and better ductility performance than that of the RC specimens. When the other parameters were the same, the larger steel tube size, the smaller shear span-to-depth ratio and the existence of studs could lead to the more satisfactory shear behavior. Then, based on the compatible truss-arch model, a set of formulas were developed to analytically predict the shear strength of the CECFST members by considering the compatibility of deformation between the truss part, arch part and the steel tube. Compared with the calculated results based on several current design specifications, the proposed formulas could get more accurate prediction.

Keywords: concrete-encased square concrete-filled steel tube members (CECFST); shear capacity; experimental study; compatible truss-arch model; calculation method

1. Introduction

Concrete-encased square concrete-filled steel tubular (CECFST) members, whose cross section consists of an interior concrete filled steel tube (CFST) and an outer reinforced concrete (RC) part, have been increasingly developed in the construction of large-scale structures and infrastructures as columns, braces or bridge piers (Han *et al.* 2014, Wang *et al.* 2020). Fig. 1 shows the construction procedure of the CECFST members in practice, which can be divided into three steps. In the first step, the square steel tube with welded shear studs and the inner high-strength concrete cores are prefabricated in factory. In the second step, after the prefabricated cores are transported to the construction site and placed in the reinforcement skeleton, the beam reinforcements can be installed, and the longitudinal rebars of RC beams can assemble outside the steel tube without intersection, which facilitates the construction process. In the third step, conventional concrete outside the core is casted to form the entire CECFST member. In the CECFST member, two different concrete materials applied in the same cross section. The high-strength concrete which was used in the prefabricated CFST core can be effectively confined by the square steel tube to improve the bearing capacity of the entire member. The conventional concrete applied in the outer part can increase the axial and lateral stiffness and provide more fire-bearing capacity under the condition of fewer material cost.

CFST members have been widely utilized due to high strength (Alatshan *et al.* 2020, Patel *et al.* 2019), well energy absorbing capacity (Al Zand *et al.* 2020, Eom *et al.* 2012), well seismic performance (Xue *et al.* 2018), and wide usage scope (Khateeb *et al.* 2020, Ekmekyapar *et al.* 2019, Zarringol *et al.* 2020, Gao *et al.* 2018). Compared with conventional CFST and RC members, the CECFST member could achieve favorable structural performance as it combines the merits of the two sections. When compared to CFST members, the CECFST members have higher fire resistance (Zhou *et al.* 2019), lateral stiffness and better durability under corrosive environment because of the existence of the outer RC. As compared with RC members, the inner CFST core provides higher bearing capacity, ductility ratio and energy absorption capacity (Zhang *et al.* 2019).

Due to the aforementioned structural advantages, the mechanical properties of the CECFST members have been studied extensively. Among them, the mechanical properties of the CECFST columns under different loading conditions were investigated (An *et al.* 2014, Han *et al.* 2014, Qian *et al.* 2016), such as axial loading, lateral loading, combined compression-torsion loading and combined compression-bend loading. Nevertheless, the nonlinear shear behavior of the CECFST members is rarely reported, and the shear failure, as a brittle failure mode, should be avoided when

*Corresponding author, Ph.D. Student
E-mail: cxsdj2019@163.com

http://www.techno-press.org/?journal=scs&subpage=8
ISSN: 1229-9367 (Print), 1598-6233 (Online)

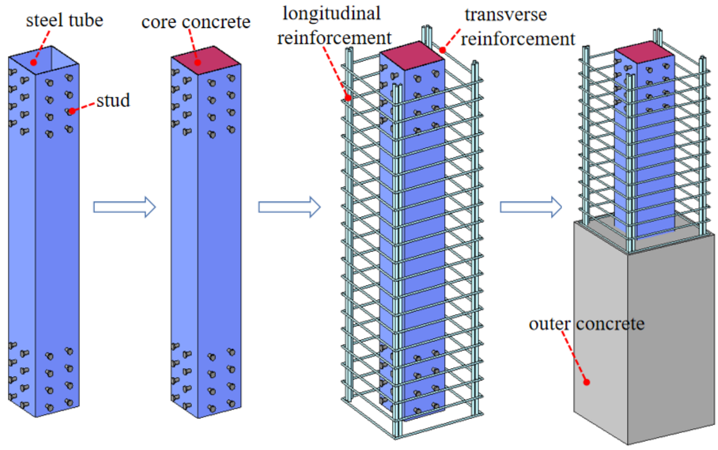

Fig. 1 Construction process of CECFST members

designing structural members.

As a conventional research method, model experiments are widely applied when investigating the shear performance of structural members. As mentioned before, the CECFST members are usually used as structural members which primarily resist the axial load, such as columns, bridge piers and braces, which are subjected to the combined effect of axial force, shear force and moment under seismic excitation. Therefore. two typical loading modes are applied when exploring the shear behavior of vertical structural members, namely, the bending-shear loading and the bending-shear-axial compression loading. The bending-shear loading mode is superior in feasibility, because the loading device and mode are conventional and accessible for most structural labs (e.g., three-point bending test or four-point bending test). Meanwhile, the bending-shear-axial compression loading is quite hard to achieve according to the lab conditions, because an additional self-balance frame is needed to apply the axial load. According to existing research, the bending-shear loading mode is usually applied when exploring the shear behavior of the structural members which suffer low axial compression (e.g. bridge piers), and the bending-shear-axial compression loading is commonly used in testing the structural members which suffer huge axial compression.

In order to avoid brittle shear failure, it is essential to predict the shear strength of the CECFST members accurately. Although the shear strengths of RC members and CFST members can be calculated based on semi-emprical formulas or mechanical models, the research regarding the calculation method for predicting the shear strength of the CECFST members is limited (Lehman *et al.* 2018, Thomas 2010). Meanwhile, it is doubtful to use the superposition method to simply combine the contribution of the RC part and the CFST part, because the compatibility of these two parts is neglected, which may lead to an overestimation of the shear strength.

In order to further explore the shear behavior of the CECFST members, in this paper, three conventional reinforced concrete (RC) members and eight CECFST members were conducted to study the failure mode, ductility and shear strength. The bending-shear loading mode was applied, and the effects of shear span-to-depth ratio, the width of inner square steel tube and shear studs of specimens were examined. The results of these parameter studies were combined with test results to develop more accurate design equations for predicting the shear resistance. Finally, a set of theoretical formulas based on the compatible truss-arch model was established to calculate the shear strength of CECFST members later in this paper.

2. Experimental investigation

2.1 Specimens details

A total of 11 specimens were fabricated and tested to investigate the shear performance under static loading. The details of specimens are shown in Table 1. In Table 1, the specimen ID denotes the specimen type + steel tube width + shear span-to-depth ratio + studs arrangement. For instance, the label C-120-1.00-s refers to the CECFST specimen, in which the cross-sectional dimension of the inner steel tube was 120 mm×120 mm, the welded studs were applied and the tested shear span-to-depth ratio was 1.0.

Fig. 2 depicts the section arrangements of the test specimens, which were similar in dimension and section shape. All of the 11 specimens had the same longitudinal and transverse reinforcements, and the cross-sectional dimension was 300 mm×300 mm. The concrete grade of the entire RC specimens and the outer part of the CECFST specimens was C30, and that of the inner part of the CECFST specimens was C80. The thickness of the concrete cover of the longitudinal reinforcements was 20 mm.

All the longitudinally reinforcing bars and stirrups were HRB335 according to GB 50917-2013, indicating that the diameter of the rebar was 20 mm and a total of 12 bars were applied in each specimen. For the stirrups, all the specimens were confined by rectangle stirrups with the diameter of 6mm. The square steel tubes were fabricated by welding together four pieces of steel plate whose grade was Q235B and the thickness was 4mm. The material properties of reinforcement and steel are summarized in Table 2. The headed shear studs were purchased from the market so that

Table 1 Details of the specimens

Specimen ID	L (mm)	a (mm)	h_0 (mm)	$\lambda=a/h_0$	d (mm)	t (mm)	Stud spacing (mm)	Loading method
RC-0-0.75-n	1350	195	260	0.75	-	-	-	4- point loading
RC-0-1.00-n	1350	260	260	1.00	-	-	-	4- point loading
RC-0-1.25-n	1350	325	260	1.25	-	-	-	3- point loading
C-120-0.75-n	1350	195	260	0.75	120	4	-	4- point loading
C-120-0.75-s	1350	195	260	0.75	120	4	@100	4- point loading
C-120-1.00-s	1350	260	260	1.00	120	4	@100	4- point loading
C-120-1.25-s	1350	325	260	1.25	120	4	@100	3- point loading
C-100-0.75-n	1350	195	260	0.75	100	4	-	4- point loading
C-100-0.75-s	1350	195	260	0.75	100	4	@100	4- point loading
C-100-1.00-s	1350	260	260	1.00	100	4	@100	4- point loading
C-100-1.25-s	1350	325	260	1.25	100	4	@100	3- point loading

Note: L is the total length of the specimen; a is the length of the shear span; h_0 is the effective depth of the section; λ is the shear span-to-depth ratio and $\lambda=a/h_0$; d and t denote the width and thickness of the square steel tube, respectively

Table 2 Mechanical properties of steel tube and reinforcements and concrete

Type	Diameter/Thickness (mm)	f_y (MPa)	f_u (MPa)	E_s (MPa)	f_{cu} (MPa)	f_c (MPa)	f_t (MPa)
Stirrup	6	425	669	209	/	/	/
Longitudinal bar	20	420	580	210	/	/	/
Steel tube	4	288	390	205	/	/	/
C30	/	/	/	/	31.8	21.3	2.33
C80	/	/	/	/	85.8	53.9	3.50

Note: f_{cu} is concrete average cubic compressive strength, f_c is concrete average prismatic compressive strength, f_t is concrete average prismatic tensile strength

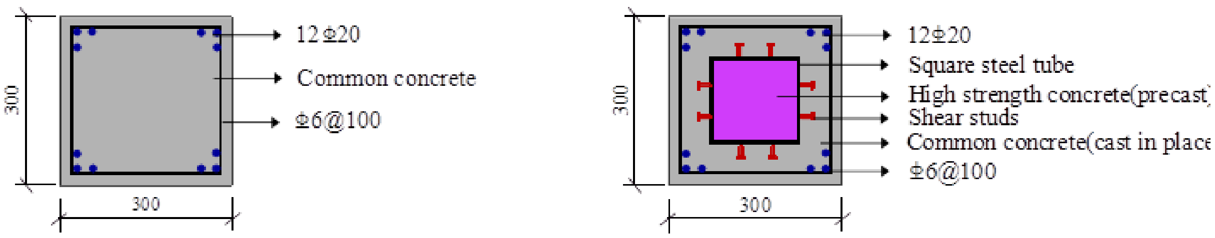

(a) Cross section of the RC member (b) Cross section of the CECFST member

Fig. 2 Cross section of the experimental specimens

the material property test of studs was not conducted. Theheight and the shank diameter of studs were 30 mm and 10 mm, respectively. The studs were spaced at 100 mm.

2.2 Material properties

Two kinds of concrete materials were used in the test specimens, namely, the grades C30 and C80. A number of

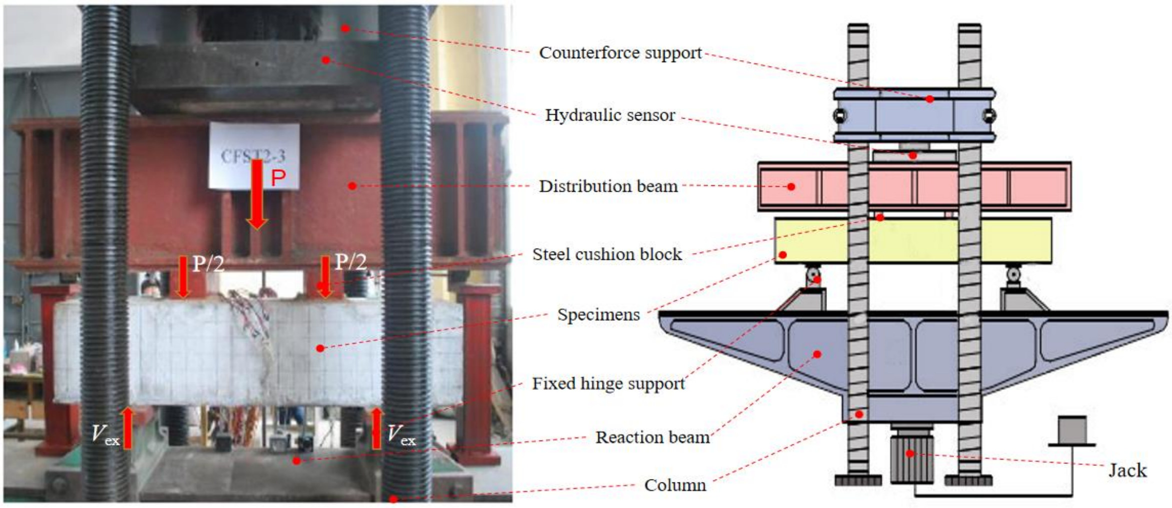

Fig. 3 The schematic view and the photo of the test device

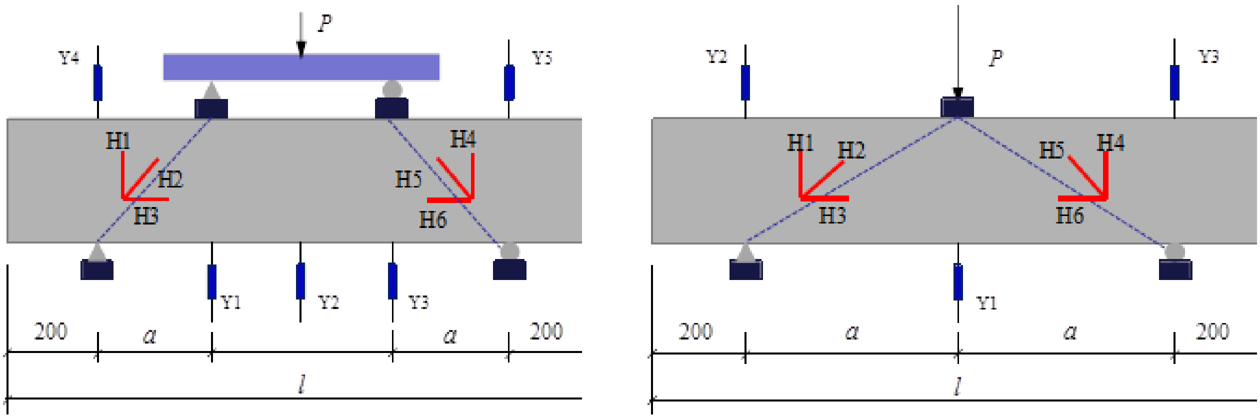

(a) Layout of four-point loading (b) Layout of three-point loading

Fig. 4 Layout of the displacement transducers and strain rosettes

concrete cubes with dimensions of 150 mm ×150 mm ×150 mm of the aforementioned two grades were casted and tested at the same time as that of the specimens. The measured concrete compressive strength are summarized in Table 2 and the concrete axial tensile strength f_t was calculated by the equation in GB 50010. Standard tensile tests were conducted per the Chinese codes to evaluate the mechanical properties of the steel tube and reinforcements, which can be also found in Table 2. Among them, elastic modulus E_s is derived from stress divided by strain and strain was simply calculated by the displacement divided by sample fixture spacing distance.

2.3 Test device

Fig. 3 shows the schematic view and the photo of the test device. In the test, the bending-shear loading was applied. All the specimens were subjected to monotonic load, which was applied by a 5000 kN electronically hydraulic testing machine. The force-displacement mixed loading mode was adopted. In the pre-loading stage, an increment of 120 kN was applied to check the normal function of the test machine. In the formal test, a vertical displacement was applied with the speed of 0.3 mm/min. Once the peak load reached, the loading speed increased to 0.5 mm/min until the load was subsequently reduced to 85% of the experimental peak load, then the test was terminated.

As indicated in Table 1, the total lengths of all the specimens were the same, and the shear span-to-depth ratio was the primary test parameter. Therefore, two different loading types, namely, the three-point loading and the four-point loading, were applied for this test program to achieve different shear span lengths, as shown in Fig. 3. During the test process, the vertical deflections of the test specimens were measured by displacement transducers, which were placed at the mid-span, the loading points and both two supports. The strains of the concrete and steel tube were monitored by strain foils or strain rosettes. The layouts of the displacement transducers and strain gauges are illustrated in detail in Fig. 4.

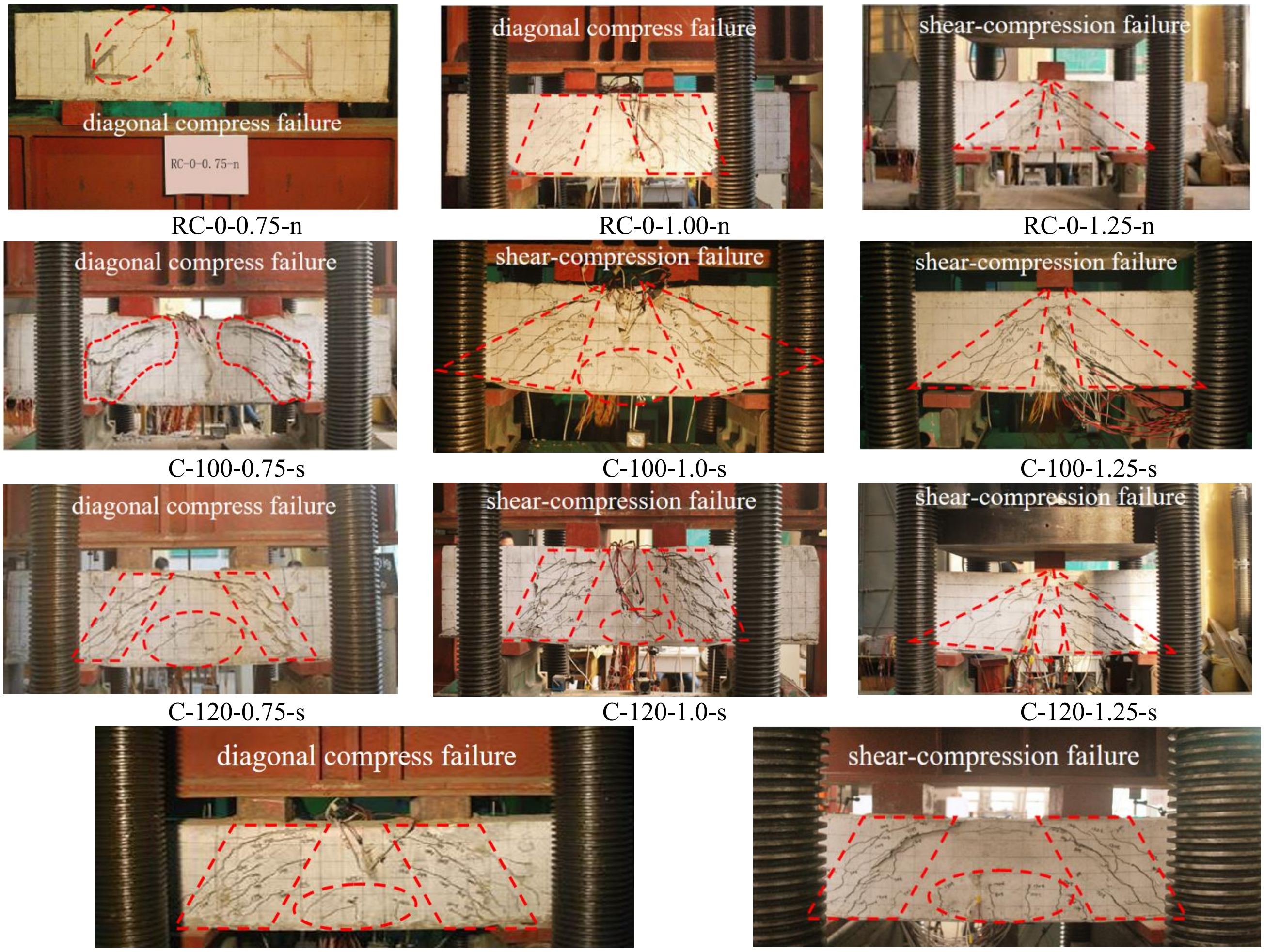

Fig. 5 Crack patterns and failure modes

3. Experimental results and discussions

3.1 Failure modes and crack patterns

Fig. 5 depicts a general view of the typical failure patterns of the specimens. From the test observations, the specimens RC-0-0.75, RC-0-1.00 and CECFST specimens with the shear span-to-depth ratio of 0.75 exhibited the typical diagonal compress failure, which can be observed as the crushing of the diagonal concrete struts. For this kind of failure, the critical oblique cracks, which were located at the member web, gradually formed with the increasing of the applied load. When the load approached the peak load, the critical oblique cracks in parallel divided the web concrete into several diagonal concrete struts, and finally the diagonal concrete struts were crushed and the specimens failed.

When shear span ratio-to-depth was greater than 0.75, the RC and CECFST specimens exhibited the shear-compression failure, indicating that the final failure occurred when the inclined cracks propagated through the section height and the top concrete was crushed. In such failure, the stirrup yielding could be observed at the intersection of the inclined crack and the stirrup when the peak load was reached, and the steel tube inside the CECFST member yielded in shear.

The crack developed process is recorded as follows. When the load reached 15%~25% P_u, the initial vertical crack appeared on the bottom part of the lateral surface at the shear span. Then the initial vertical crack extended forward to the adjacent loading point and an oblique crack formed, followed by a vertical bending crack observed at the mid-span. When the load reached 50%~70% P_u, the crack spacing gradually stabilized and the cracks at the shear span redirected and stretched to the loading points. Then the inclined crack band extended to the surface of the steel tube. During this period, the vertical cracks in the mid-span developed slowly, while the inclined cracks at the shear span developed rapidly. When the peak load was approached, the concrete at the shear span bulged obviously accompanied by spalling, and then the major inclined cracks formed. Finally, the crushing of the top concrete was observed and the specimen failed.

During the testing process, some longitudinal cracks appeared along the steel tube at the both ends of the CECFST members with no studs, but these cracks did not develop. It indicated that there was a slight slippage between the steel tube and the adjacent concrete, which

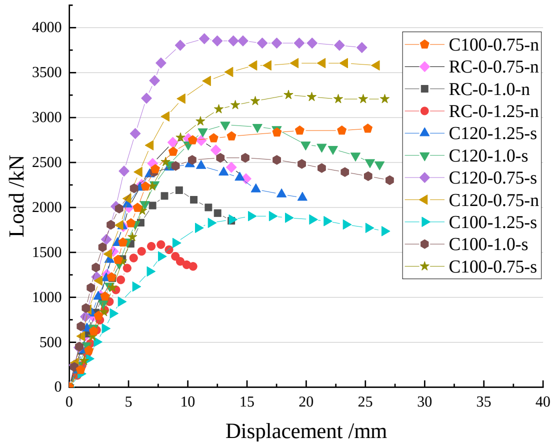

Fig. 6 Load-displacement curves of all specimens

Table 3 Summary of test results

Specimen ID	P_{cr} (kN)	Δ_y (mm)	P_y (kN)	Δ_u (mm)	$\mu=\Delta_u/\Delta_y$	P_u (kN)
RC-0-0.75-n	670	7.42	2346	14.88	2.01	2760
RC-0-1.00-n	540	6.99	1875	13.66	1.95	2206
RC-0-1.25-n	470	5.89	1338	10.34	1.76	1574
C-120-0.75-n	700	9.49	3062	25.85	2.72	3268
C-120-0.75-s	1100	7.82	3283	23.58	3.02	3863
C-120-1.00-s	500	9.68	2226	26.09	2.70	2619
C-120-1.25-s	430	6.57	2112	19.57	2.98	2485
C-100-0.75-n	740	9.31	2364	25.33	2.72	2782
C-100-0.75-s	640	11.34	2875	26.78	2.36	3382
C-100-1.00-s	440	5.61	1947	27.02	4.82	2290
C-100-1.25-s	480	10.37	1615	26.62	2.57	1900

implied that the inter CFST core and outer concrete behaved as an integral member even without studs.

3.2 Load-displacement curves

The load-displacement curves of all the specimens are displayed in Fig. 6. For the RC members, the load decreased rapidly after the experienced peak load reached, indicating that the brittle failure occurred. After the peak load of the CECFST specimens reached, the load-displacement curves declined slightly. The platform or the slight decline of the post-peak period showed in the load-displacement curves indicated that the CECFST members could exhibit excellent deformability because of the favorable plastic performance of the internal CFST core

The load-displacement curves of the RC series, C-120 series, C-100 series are compared in Fig. 8, whilst the further comparison of the test specimens are shown in Table 3. In Table 3, the main results including the cracking load P_{cr}, yield load P_y, ultimate load P_u, yield deflection Δ_y, ultimate deflection Δ_u and ductility coefficient μ. The ductility coefficient was calculated according to the equivalent elasto-plastic energy method. According to the test and analysis results, the bearing capacity and deformability of the CECFST specimens were higher than those of the RC specimens. Based on the curves and test results, main conclusions can be drawn as follows.

(1) The shear capacity of test specimens was effected by the following four reasons, the existence of the inner CFST core, the shear span-to-depth ratio, the steel tube dimension and the studs arrangement. The increase of the steel tube size exhibited the largest contribution to the shear capacity.
(2) The load of the RC members fell rapidly after the peak load reached, but the CECFST specimens could effectively maintain the peak load in the post-peak period and the curve declined slowly. The average ductility coefficient of the CECFST series was 5.6% higher than that of the RC series, indicating that all the CECFST composite specimens had great deformability, which mainly attributed to the constraint effect of the steel tube on the internal high strength concrete.
(3) With the increase of the shear span-to-depth ratio, the

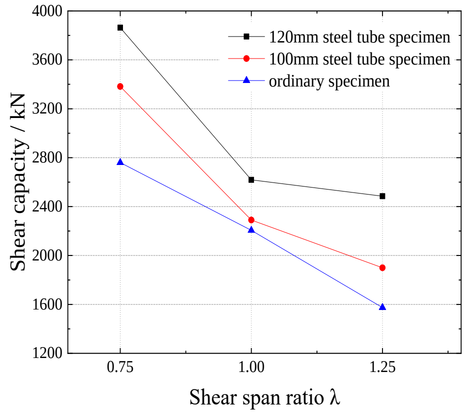

Fig. 7 Influence of shear span-to-depth ratios on shear capacity

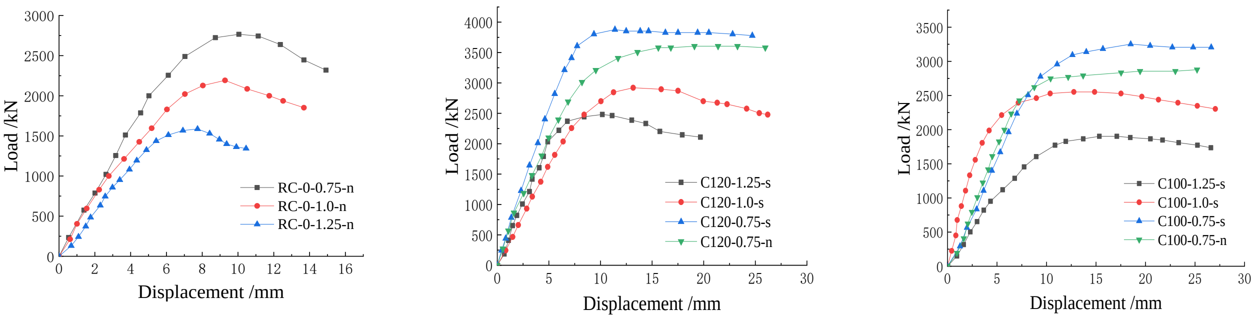

(a) RC series (b) C-120 series (c) C-100 series

Fig. 8 Load-displacement curves of three series under different span-to-depth ratios

shear capacity of the specimens decreased, while the ductility did not decrease significantly in the CECFST series as shown in Fig. 8.

(4) The shear capacity of the specimens with studs increased slightly and similar ductility of that compared with those with no studs.

3.2.1 Effect of shear span-to-depth ratio

The relationship of the shear span-to-depth ratio and the shear capacity of the RC specimens and the CECFST specimens was displayed in Fig. 7. The load- displacement curves of the three series with different shear span-to-depth ratios were compared in Figs. 8(a)-8(c). The development trend of the shear capacity for RC series was similar to that of the CECFST series specimens, namely, the shear capacity decreased with the increase of the shear span-to-depth ratio. However, as the size of the steel tube increased, the influence of the shear span-to-depth ratios on the bearing capacity gradually diminished.

According to the failure modes and load- displacement curves, the shear span-to-depth ratio directly effected the failure modes. As shown in Fig. 5, if the shear span-to-depth ratio was less than 1.0, the diagonal compression failure occurred. When the shear span ratio-to-depth was more than 1.0, the shear-compression failure was observed. However, it should be noticed that the finally failure of the CECFST specimens was ductile, although the CECFST specimens had the similar failure phenomena when shear span-to-depth ratio was 0.75. Because of the plasticity of the internal steel tube after yielding, the shear capacity and ductility were both superior when the shear span-to-depth ratio of the specimen was 0.75.

3.2.2 Effect of steel tube width

Fig. 9 illustrates a positive correlation between the shear capacity and the steel tube width. The CECFST specimens with the tube width of 100 mm exhibited an increase of 19.6% on the average shear capacity compared with that of the RC members, while the CECFST specimens with the tube width of 200 mm exhibited an increase of 23.8% on the average shear capacity compared with that of those with the tube width of 100 mm. The reason why the improvement trend is similar was that with the increase of the width of the steel tube, the constraint effect of the steel tube on the internal high strength concrete increased.

The load-displacement curves of the three types of the test specimens under the same shear span-to-depth ratio were compared in Figs. 10(a)-10(c). The effect of the internal steel tube on the shear behavior can be concluded as follows. When steel tube width grew, the stiffness in the early loading stage increased, so the displacement at the yield strength was small, besides the ultimate displacement decreased. It can be seen that the overall ductility increased with the increase of the steel tube size. However, the section

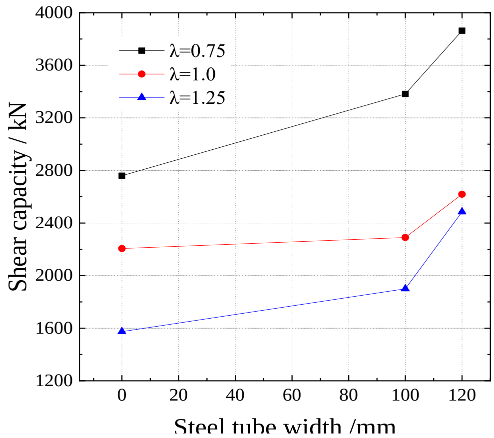

Fig. 9 Influence of steel tube width on shear capacity

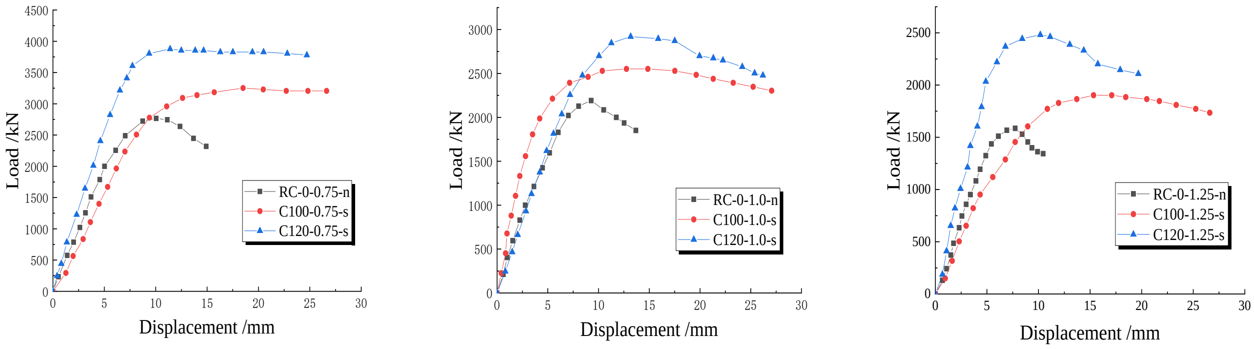

(a) Shear span ratio is 0.75 (b) Shear span ratio is 1.0 (c) Shear span ratio is 1.25

Fig. 10 Load-displacement curves of three series under different steel tube width

size of the steel tube cannot be too large, because bonding cracks along the contact point of steel tube and outer concrete might appear and affect the bearing capacity, which can be seen on outer concrete surface along the steel tube at the specimen ends.

3.2.3 Effect of shear studs

It can be derived from Fig. 8 that the effect of shear studs on the shear capacity of the CECFST specimens. The shear strengths of the specimens C-120-0.75-s and C-120-0.75-n were 3863 kN and 3268 kN. The shear strength of C-120-0.75-s was 18.2% higher than that of C-120-0.75-n, while the shear strength of C-100-0.75-s was 21.6% higher than that of C-100-0.75-n. For the specimens without shear studs, although the slight cracks along the edge of the steel tube occurred during the loading process, the bond failure did not occur. For the specimens with shear studs, no obvious longitudinal cracks were observed at the edge of the steel tube. The improvement on the shear capacity of the CECFST members with shear studs may be attributed to the composite action provided by the studs. Although there was no bond failure of the specimens without studs, it is still recommended to apply shear studs for safety and higher capacity.

4. The calculated methods in specification for shear strength

At present, there are few specification like the CECS 188:2005, which can be used to calculate CECFST members. However, the shear behavior of the CECFST members is similar to that of the shape steel reinforced concrete (SRC) members, the shear capacity of the CECFST members can be also estimated by the relevant design codes regarding SRC members. As shown in Table 4, almost all of the current design codes accept the concept of strength superposition for the analysis and design of SRC members, that is, the shear strength of SRC members can be obtained as the sum of the shear strength of the reinforced concrete (RC) and that of the steel tube part. The superposition is simple and feasible for structural engineers in practical applications. However, there are some differences in various calculation methods. The design formulas of the codes JGJ 138, YB 9082 and CECS 188 are similar, although some coefficients are different (Xue *et al.* 2020, Li *et al.* 2017, CECS 188:2005, AISC 360-16, EC 2 and EC 3). The code GB 50936 used a unified theory to calculate the bearing capacity of CFST members under single load or complex loads, and the formulas are suitable for different section shape of specimens. The code AISC 360-16 only considers the shear strength of the steel tube

Table 4 Existing shear strength formulas for steel reinforced concrete members

Code	V_c	V_s	V_{ss}	$V_u = V_c + V_s + V_{ss}$
JGJ 138-2016	$\frac{1.75}{\lambda+1.0} f_t b h_0$	$\frac{f_{yv} A_{sv} h_0}{s}$	$\frac{0.58}{\lambda} f_{ss} t_w h_w$	(1)
YB 9082-2006	$\frac{1.75}{\lambda+1.0} f_t b h_0$	$\frac{f_{yv} A_{sv} h_0}{s}$	$\frac{A_w f_{ss}}{\sqrt{3}}$	(2)
CECS 188:2005	$\frac{1.75}{\lambda+1.0} f_t b h_0$	$\frac{f_{yv} A_{sv} h_0}{s}$	$\frac{2.5}{\sqrt{(1+4\lambda^2)}} f_{ss} A_w$	(3)
GB 50936—2014		$1.083\times f_{ss} \frac{\alpha}{\alpha+1} \times A_{sc}$		(4)
AISC 360-16	-	$\frac{f_{yv} A_{sv} h_0}{s}$	$0.6\varphi_v f_{ss} A_w C_v$	(5)
EC 2 and EC 3	$0.18k\left(100\rho_s f_c^{'}\right)^{\frac{1}{3}} b h_0$	$0.9 f_{yw} \frac{A_{sv}}{s} h_0 \cot\theta$	$\frac{A_w f_{ss}}{\sqrt{3}}$	(6)

Note: V_c is the shear strength provided by concrete; V_s is the shear strength provided by stirrups; V_{ss} is the shear strength provided by steel; V_u is the summary shear strength of the above three parts

and ignores the contribution of concrete. The design formula of the code EC 2 and EC 3 can be also divided into four parts, but the calculation formula is different from other design codes.

In Table 4, f_c is the cubic axial compressive strength of concrete; f'_c is the cylinder compressive strength of concrete; f_t is the axial tensile strength of concrete; b is the width of members; h_0 is the section effective height; f_y, A_{sv}, ρ_s are the yield strength, sectional area, spacing and reinforcement ratio of stirrup, respectively; f_{ss}, t_w, h_w, A_w denote the yield strength, thickness, height and area of steel web plate; α is the sectional steel ratio and A_{sc} is the total section area of the steel tube and concrete; φ_v and C_v are two strength factors.

The calculation results using the aforementioned formulas are shown in Table 5. The mean value and the coefficient of variation are shown in Fig. 19, which indicates that the calculated values are conservative compared with the test results because of the employment of the safety coefficient in the design specifications.

5. Proposed formulas for shear strength

In order to simplify the analysis, the shear capacity of the CECFST members can be assumed to be composed of the reinforced concrete part and the steel tube part, as shown in Fig. 11, and the entire shear capacity is the superposition of these two parts.

Up to now, the shear mechanism of the reinforced concrete members mainly consists of the truss theory, ultimate failure theory, nonlinear finite element theory, strut and tie model theory. In this paper, the truss-arch model is used to analyze the shear mechanism of the CECFST members on the basis of the truss theory and arch theory.

In the truss-arch model, two different actions are assumed to resist the vertical shear force, namely, the truss action and the arch action. When the shear span-to-depth ratio is small, the arch action is the main resistance and the contribution of the truss action is little. When the shear span-to-depth ratio is large, the truss action governs. Before the cracks appear, the shear force is mainly transferred through the concrete in the arch model and the concrete behaves as compressive struts, as shown in Fig. 11(a). After the occurrence of diagonal cracks, the shear stress is redistributed and the stirrups begin to bear more shear force. At this time, the concrete between the up and bottom longitudinal reinforcements forms the secondary compressive struts, which forms an ideal truss model, as shown in Fig. 11(b). Therefore, the contribution of the reinforced concrete part on the shear strength of the entire CECFST member is provided by the compressive concrete struts and the truss analogy.

Based on the above analysis, the shear behavior of the CECFST members can be described by coupling the steel tube part and the reinforced concrete part. The shear strength of the RC part is considered as the combination of the truss action V_t and the arch action V_a, and the contribution of the steel tube to shear capacity is V_s. The calculation diagrams of the aforementioned three parts are shown in Fig. 12. Considering the condition of deformation compatibility, the shear deformation induced by the truss-arch part must be equal to that induced by the steel tube part, where K_t, K_a, K_s denote the shear stiffness of the truss part, arch part and steel tube, respectively.

5.1 Basic assumptions

The following basic assumptions were made.

(1) The tensile strength of concrete is neglected.

(2) The dowel action is ignored in the calculation model,

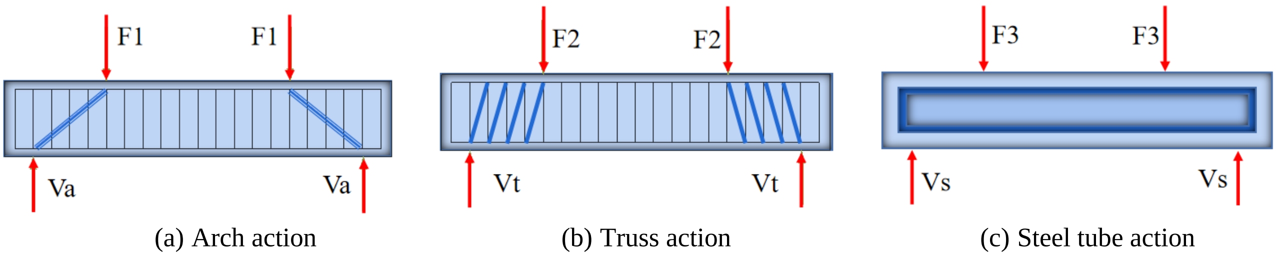

Fig. 11 Action decoupling

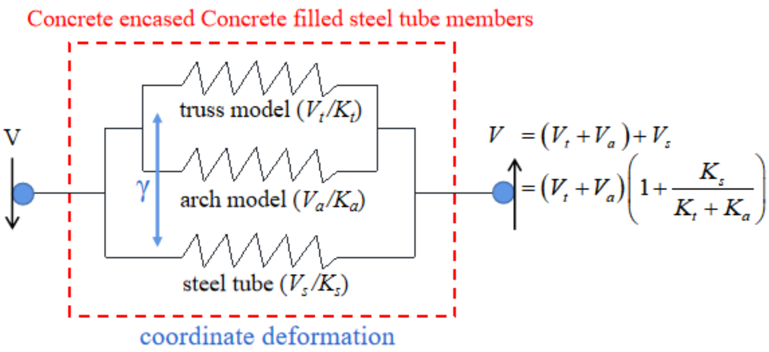

Fig. 12 Calculation diagram

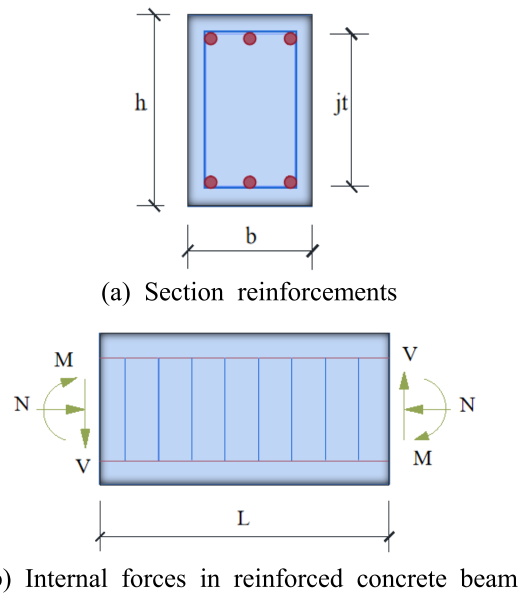

Fig. 13 Section reinforcements and internal forces in RC part

and the stirrups are considered to have yielded when the member reaches the peak load.

5.2 Shear strength of the reinforced concrete part

According to Aoyama (1993), who explains the shear calculation method applied in AIJ, the shear strength of the RC member consists of the truss action and the arch action. The arrangement of steel reinforcements in the cross section and the internal forces in RC part are shown in Fig. 13.

5.2.1 Arch action V_a

The arch action V_a is assumed to be a single compressive strut directed from the compression zone at the top toward that at the bottom, as shown in Fig. 14, where the strut top is the loading point and the strut bottom is the support, and L is the distance between the two loading

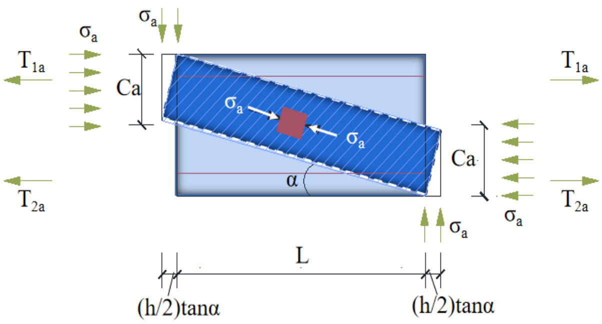

Fig. 14 Arch model

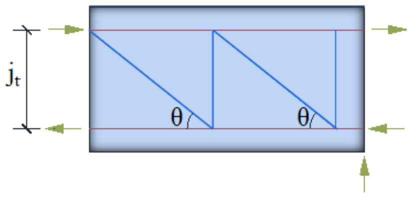

(a) Truss action

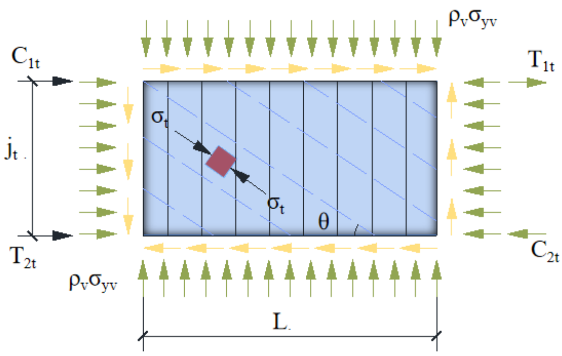

(b) Free body diagram of truss action

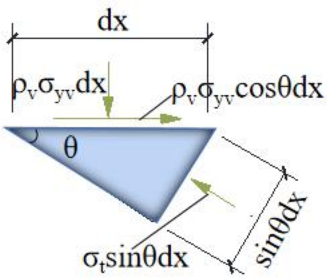

(c) Portion of truss action along a crack

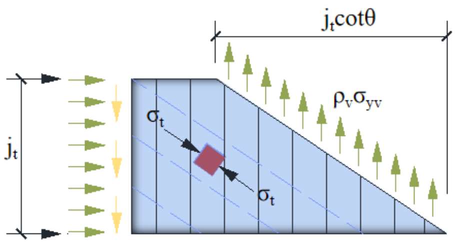

(d) Equivalence of stresses acting on an element

Fig. 15 Truss model

points. The angle between the compressive concrete strut and the axis is α. The effective depth of the compressive arch is C_a, and a parameter k is employed here (Hsu *et al.* 2010) to evaluate the effective depth, as shown in Eq. (7).

In the arch model, the shear capacity V_a can be concluded

$$V_a = b \cdot C_a \cdot \sigma_a \cdot tan\alpha \tag{7}$$

$$\tan\alpha = \frac{h}{l} \tag{8}$$

$$C_a = kh \tag{9}$$

$$k = \sqrt{\left[n\rho + (n-1)\rho'\right]^2 + 2\left[n\rho + (n-1)\rho' d'/d\right]} - \left[n\rho + \left(n-1\right)\rho'\right] \tag{10}$$

Where σ_a is the axial compressive stress of the compressive arch; h is the cross-sectional height.

5.2.2 Truss action V_t

In the experiment, the diagonal cracks did not develop in parallel. To simplify the calculation process, it can be assumed that the inclinations of the diagonal struts are equal. The simplified truss model is shown in Figs. 15(a), and the free body diagram of the truss action is illustrated in and 15(b). In the truss model, the bottom longitudinal reinforcements are the tensile chords, the top compressive concrete and the longitudinal bars can be regarded as the compressive chords; the stirrups are the web chords in the truss model. Average compressive stress of diagonal strut σ_t can be calculated using Eq. (11) according to the balance condition of the top reinforcement, as shown in Fig. 15(c).

$$\sigma_t = \frac{\rho_v \sigma_{yv}}{\sin^2\theta} = \rho_v \sigma_{yv}\left(1+\cot^2\theta\right) \tag{11}$$

The shear strength provided by the truss action V_t is derived from the balance of the vertical force as shown in Fig. 15 (d).

$$V_t = bj_t \rho_v \sigma_{yv} \cot\theta \tag{12}$$

where ρ_v is the stirrup ratio; σ_{yv} is the stirrup yield strength; j_t is the distance between the top and bottom longitudinal reinforcements; θ is the inclination of the compressive strut in the truss model.

5.2.3 The total shear strength of reinforced concrete V_u

The shear capacity of the RC part can be obtained by combining the shear capacities of the truss and the arch action, as shown in Eq. (13).

$$\begin{aligned} V_u &= V_t + V_a \\ &= bd_v \rho_v \sigma_{yv} \cot\theta + b \cdot C_a \sigma_a \tan\alpha \end{aligned} \tag{13}$$

When the stress of the stirrups reach to their yield strength, namely, $\sigma_{yv}=f_{yv}$ and the diagonal concrete struts attain their compressive strength, the member will achieve the shear capacity. Due to the different strengths of the concrete inside and outside the steel tube, the compressive strength of the concrete f_c can be evaluated by the weighted areas of the inner part and the outer part. A parameter β is proposed to considered the strength reduction of the concrete due to the softening. Therefore, the shear capacity of the RC part can be determined by Eq. (16).

$$\sigma_t + \sigma_a = \gamma_0 f_c \tag{14}$$

$$\beta = \frac{\sigma_t}{\gamma_0 f_c} = \frac{\rho_v \sigma_{yv}\left(1+\cot^2\theta\right)}{\gamma_0 f_c} \tag{15}$$

$$\begin{aligned} V_u &= V_t + V_a \\ &= bj_t \rho_v f_{yv} \cot\theta + b \cdot C_a (1-\beta)\gamma_0 f_c \tan\alpha \end{aligned} \tag{16}$$

5.3 Stiffness calculation of reinforced concrete and steel tube

In order to meet the requirement of deformation compatibility, the shear stiffness of the RC part and that of the steel tube should be evaluated using comprehensive models.

5.3.1 Shear stiffness of truss model

Fig. 16 indicates that the shear deformation of the truss action is mainly produced by the compression of the concrete strut and the elongation of the stirrups, respectively (Pan *et al.* 2013). Therefore, the shear stiffness of the truss model is shown in Eq. (18). The expression for θ (Kim and Mander 1999) is expressed as follows.

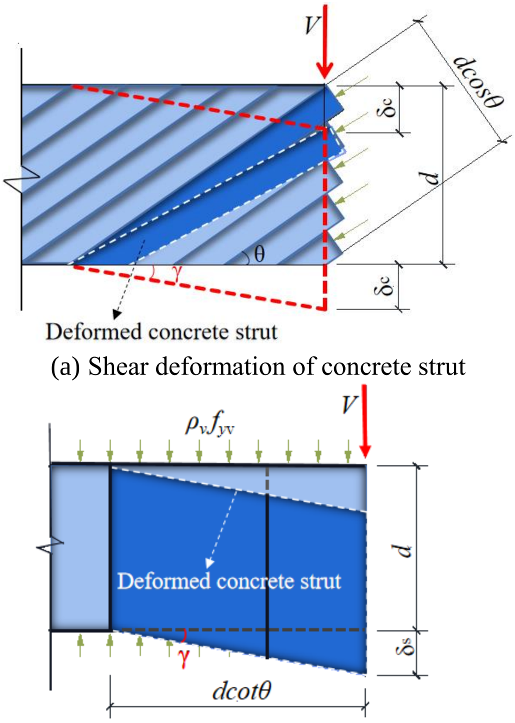

Fig. 16. Shear deformation of truss section

$$\theta = \arctan\left(\frac{n\rho_v + \zeta_2 \dfrac{\rho_v b j_t}{A_s}}{1+n\rho_v}\right)^{1/4} \tag{17}$$

where n is the ratio of elastic modulus of steel to concrete; ζ_2 =0.57; A_s is the cross-sectional area of the longitudinal reinforcements.

$$\begin{aligned} K_t &= \frac{V}{\left(\dfrac{\delta_s+\delta_c}{d\cot\theta}\right)} \\ &= \frac{V}{\left(\dfrac{V}{E_c b j_t \sin^2\theta\cos^2\theta}\right)+\left(\dfrac{V}{E_s\rho_v b\cot^2\theta}\right)} \\ &= \frac{n\rho_v E_c b j_t \cot^2\theta}{1+n\rho_v \csc^4\theta} \end{aligned} \tag{18}$$

5.3.2 Shear stiffness of arch model

The shear deformation of the arch model is induced by the compression of the concrete arch, as shown in Fig. (17). Therefore, the shear stiffness of the arch model is shown in Eq. (18).

$$K_a = \frac{V}{\gamma_a} = \frac{V}{\delta_a / l} = E_c b c_a \cos^2\alpha \sin^2\alpha \tag{19}$$

Table 5 Validation

Specimen ID	Test value V_{ex} (kN)	Proposed model V_{ca1} (kN)	Calculated results using different codes (kN) V_1	V_2	V_3	V_4	V_5	V_6	Comparison $\frac{V_{cal}}{V_{ex}}$	$\frac{V_{c1}}{V_{ex}}$	$\frac{V_{c2}}{V_{ex}}$	$\frac{V_{c3}}{V_{ex}}$	$\frac{V_{c4}}{V_{ex}}$	$\frac{V_{c5}}{V_{ex}}$	$\frac{V_{c6}}{V_{ex}}$
C-120-0.75-n	1634	1647	535	598	705	586	277	422	1.01	0.33	0.37	0.43	0.36	0.17	0.26
C-120-0.75-s	1932	1647	535	598	705	586	277	422	0.85	0.28	0.31	0.36	0.30	0.14	0.22
C-120-1.00-s	1310	1283	457	574	606	586	277	422	0.98	0.35	0.44	0.46	0.45	0.21	0.32
C-120-1.25-s	1243	1089	406	554	535	586	277	422	0.88	0.33	0.45	0.43	0.47	0.22	0.34
C-100-0.75-n	1391	1463	500	552	641	490	252	396	1.05	0.36	0.40	0.46	0.35	0.18	0.28
C-100-0.75-s	1691	1463	500	552	641	490	252	396	0.86	0.30	0.33	0.38	0.29	0.15	0.23
C-100-1.00-s	1145	1149	431	527	555	490	252	396	1.00	0.38	0.46	0.48	0.43	0.22	0.35
C-100-1.25-s	950	979	385	508	492	490	252	396	1.03	0.41	0.53	0.52	0.52	0.27	0.42
Mean value									0.96	0.34	0.41	0.44	0.40	0.20	0.30
Standard deviation									0.08	0.04	0.07	0.05	0.08	0.04	0.07
Variable coefficient									0.08	0.12	0.18	0.12	0.21	0.21	0.22

Note: V_{cal} is the result calculated using the proposed formula; V_1~V_6 correspond to the formulas Eq.(1)~Eq.(6).

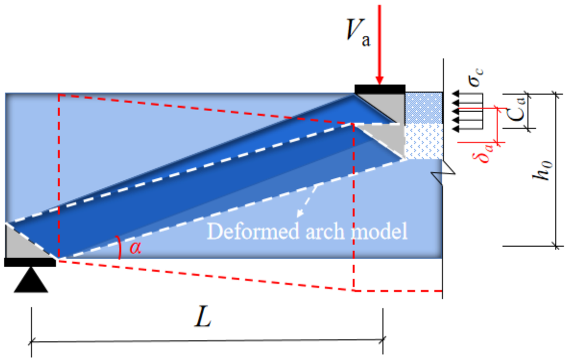

Fig. 17 Shear deformation diagram of arch model

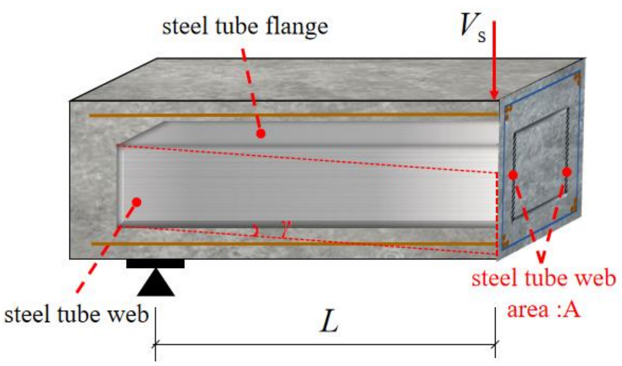

Fig. 18 Shear deformation diagram of steel tube

5.3.3 Shear stiffness of steel tube

The diagram multiplication method is used to calculate the shear deformation of the steel tube, as shown in Fig. 18. The detailed equation is recorded in Eq. (20), where G is the shear modulus of steel; A is the web area of the steel tube.

$$K_s = \frac{V}{\gamma} = \frac{V}{\delta_s / l} = GA \tag{20}$$

5.4 Calculation methods and validation

To conclude, Eq. (21) is applied here to calculate the shear strength of a CECFST member. In Eq. (21), the RC part and the steel tube are related using shear stiffness, indicating that the deformation compatibility between these two parts are achieved.

Table 5 represents the measured shear capacity of the specimens in the test as well as the calculation results according to the proposed formulas and several design specifications.

$$V = (V_t + V_a) + V_s = (V_t + V_a)\left(1 + \frac{K_s}{K_t + K_a}\right) \tag{21}$$

As shown in Fig. 19, the results calculated using the proposed method agree well with the tested shear capacities of the CECFST members. The mean value of the calculated values to the test values is 0.96, and the standard deviation is 0.08, and the coefficient of variation is 8%. Meanwhile,

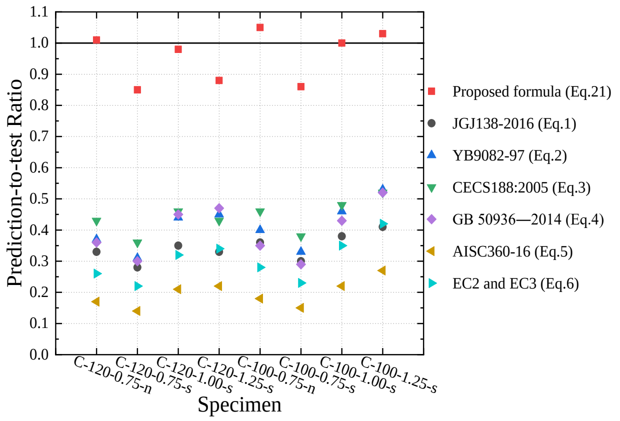

Fig. 19 Scatter of prediction-to-test ratios by different equations

the results calculated in terms of the current design codes are too conservative, because of the reliability requirements in codes.

6. Conclusions

This paper presents the experiments and theoretical analysis on the shear capacity of square CECFST members subjected to static loading. Three RC and eight CECFST specimens were tested to investigate the effects of the shear span-to-depth ratio, arrangement of shear studs and the size of steel tube on the shear behavior. Based on the experimental results, the main conclusions could be drawn as follows.

(1) All the test specimens failed in shear. Among them, the CECFST specimens exhibited higher shear strength and displacement ductility than RC specimens because of the existence of the CFST core. When the other parameters were the same, the increase of the steel tube and the application of shear studs could lead to more satisfactory shear behavior.

(2) The shear strength decreases with the increase of the shear span-to-depth ratio, and the shear capacity of specimens is directly effected by the steel tube width. The shear capacity of the CECFST specimens with the steel tube width of 100 mm was 19.6% higher than that of RC members, and 56.6% lower than that of the CECFST specimens with the tube width of 200 mm.

(3) It is recommended to use the shear studs on the steel tube, because studs can slightly improve the shear capacity of specimens according to the experimental results. There was no obvious bond cracks observed on the CECFST specimens, which indicated that the internal CFST core had good composite action with outside RC.

(4) Based on the compatible truss-arch model, a set of formulas were developed to analytically predict the shear strength of the CECFST members by considering the compatibility of deformation between the truss part, arch part and the steel tube. Compared with the calculated results based on several current design codes, the proposed formulas could get the most accurate prediction.

Above all, the CECFST specimens represented well shear capacity and ductility. In order to control the development of shear cracks and avoid brittle failure, the spacing and sectional area of constructional steel reinforcement could be small and large respective within the scope specified in the code. The further bending experiment can explore the distance between support and first crack start point, which can be used to provide the first stirrup in the members. (Choi *et al.* 2007)

Acknowledgments

This work was supported by the National Natural Science Foundation of China (Program No. 51578443).

References

ACI 318 (2014), Building Code Requirements for Structural Concrete and Commentary; American Concrete Institute, USA.

Alatshan, F., Osman, S.A., Mashiri, F. and Hamid, R. (2020), "Explicit simulation of circular CFST stub columns with external steel confinement under axial compression", *Materials*, **13**(1), https://doi.org/10.3390/ma13010023.

Al Zand, A.W., Badaruzzaman, W.H.W. and Tawfeeq, W.M. (2020), "New empirical methods for predicting flexural capacity and stiffness of CFST beam", *J. Constr. Steel Res.*, **164**(1), 105778.1-105778.15. https://doi.org/10.1016/j.jcsr.2019.105778.

An, Y.F. and Han, L.H. (2014), "Behaviour of concrete-encased CFST columns under combined compression and bending", *J. Constr. Steel Res.*, **101**, 314-330.

Aoyama, H. (1993), "Design philosophy for shear in earthquake resistance in Japan", https://doi.org/10.1016/j.jcsr.2014.06.002.

ASIC 360 (2016), Specification for structural steel buildings, American Institute of Steel Construction; Chicago, USA.

CECS 188:2005 (2005), Technical Specification for Steel Tube Reinforced Concrete Column Structure, China Planning Press; Beijing, China.

Choi, K.K., Park, H.G. and Wight, J.K. (2007), "Unified shear strength model for reinforced concrete beams-Part I: Development", *ACI Struct. J.*, **104**(2),142-152.

Choi, K.K. and Park, H.G. (2007), "Unified shear strength model for reinforced concrete beams-Part II: Verification and simplified method", *ACI Struct. J.*, **104**(2), 153-1 61.

Ekmekyapar, T., Alwan, O.H., Hasan, H.G., Shehab, B.A. and Al-Eliwi, B.J.M. (2019), "Comparison of classical, double skin and double section CFST stub columns: experiments and design formulations", *J. Constr. Steel Res.*, **155**(4), 192-204. https://doi.org/10.1016/j.jcsr.2018.12.025.

Eom, S.S., Vu, Q.V. and Choi, J.H., Papazafeiropoulos, G. and Kim, S.E. (2019), "Behavior of composite CFST beam-steel column joints(Article)", *Steel Compos. Struct.*, **32**(5), 583-594. https://doi.org/10.12989/scs.2019.32.5.583.

Eurocode 2 (1992), Design of concrete structures - Part 1 : General rules and rules for Buildings. European Committee for Standardization ; Brussels, European.

Eurocode 3 (2005), Design of steel structures - Part 1-1 : General rules and rules for Buildings. European Committee for Standardization; Brussels, European.

GB 50010-2010. Code for design of concrete structures, Ministry of Construction of China, Beijing, China; 2010 [in Chinese].

GB 50917-2013. Code for Design of Steel and Concrete Composite Bridges, Ministry of Construction of China, Beijing, China; 2013 [in Chinese].

Gao, D.Y., You, P.B., Zhang, L.J. and Yan, H.H. (2018), "Seismic behavior of SFRC shear wall with CFST columns". *Steel Compos. Struct.*, **28**(5), 527-539. https://doi.org/10.12989/scs.2018.28.5.527.

Han, L.H., Li, W. and Bjorhovde, R. (2014), "Developments and advanced applications of concrete-filled steel tubular (CFST) structures: members", *J. Constr. Steel Res.*, **100**(9), 211-228. https://doi.org/10.1016/j.jcsr.2014.04.016.

Han, L.H. and An, Y.F. (2014), "Performance of concrete-encased CFST box stub columns under axial compression", *J. Constr. Steel Res.*, **93**(2), 62-76. https://doi.org/10.1016/j.jcsr.2013.10.019.

Hsu, T.T.C. and Mo, H.Y.L (2010), "Unified Theory of Concrete Structures", *Wiley*. https://doi.org/10.1002/9780470688892

Khateeb, B.M., Siddiqui, N.A., Almusallam, T.H., Abbas, H. and Al-Salloum, Y.A. (2020), "Behavior of novel CFST circular column-to-foundation connections under cyclic loading", *Eng. Struct.*, **221**, 111051. https://doi.org/10.1016/j.engstruct.2020.111051.

Kim, J.H. and Mander. J.B. (1999), "Truss modeling of reinforced concrete shear-flexure behavior", *Multidisciplinary Center for Earthquake Engineering Research*, Buffalo, USA.

Lehman, D., Roeder, C., Heid, A., Maki, T. and Khaleghi, B. (2018), "Shear response of concrete filled tubes part 1: experiments", *J. Constr. Steel Res.*, **150**(11), 528-540. https://doi.org/10.1016/j.jcsr.2018.08.027.

Li, W., Xu, L.F. and Qian, W.W. (2019), "Seismic performance of concrete-encased CFST column to steel beam joints with different connection details", *Eng. Struct.*, **204**, 109875. https://doi.org/10.1016/j.engstruct.2019.109875.

Pan, Z. and Li, B. (2013), "Truss-arch model for shear strength of shear-critical reinforced concrete columns", *J. Struct. Eng.*, **139**(4), 548-560. https://doi.org/36.10.1061/(ASCE)ST.1943-541X.0000677.

Patel, V.I., Hassanein, M.F., Thai, H.T., Abadi, H.A., Elchalakani, M. and Bai, Y. (2019), "Ultra-high strength circular short CFST columns: axisymmetric analysis, behaviour and design", *Eng. Struct.*, **179**(1), 268-283. https://doi.org/10.1016/j.engstruct.2018.10.081.

Qian, W.W., Li, W., Han, L.H. and Zhao, X.L. (2016), "Analytical behavior of concrete-encased CFST columns under cyclic lateral loading", *J. Constr. Steel Res.*, **120**(4), 206-220. https://doi.org/11.10.1016/j.jcsr.2015.12.018.

Xue, J., Zhou, C. and Lin, J. (2018), "Seismic performance of mixed column composed of square CFST column and circular RC column in Chinese archaized buildings", *Steel Compos. Struct.*, **29**(4), 451-464. https://doi.org/10.12989/scs.2018.29.4.451.

Xue, Y.C., Yang, Y. and Yu, Y.L. (2020), "Shear strength model for steel reinforced concrete composite members: Short columns and deep beams", *Eng. Struct.*, **216**, 110748. https://doi.org/10.1016/j.engstruct.2020.110748.

YB 9082-2006. Technical specification of steel-reinforced concrete structures. Beijing: Metallurgical Industry Press; 2006.

Zarringol, M., Thai, H.T., Ngo, T. and Patel, V. (2020), "Behaviour and design calculations of rectangular CFST beam-columns with slender sections", *Eng. Struct.*, **222**, 111142. https://doi.org/10.1016/j.engstruct.2020.111142.

Zhang, J., Li, X., Cao, W. and Yu, C. (2019), "Cyclic behavior of steel tube-reinforced high-strength concrete composite columns with high-strength steel bars", *Eng. Struct.*, **189**(6), 565-579. https://doi.org/17.10.1016/j.engstruct.2019.04.006.

Zhou, K. and Han, L.H. (2019), "Modelling the behaviour of concrete-encased concrete-filled steel tube (CFST) columns subjected to full-range fire", *Eng. Struct.*, **183**, 265-280. https://doi.org/10.1016/j.engstruct.2018.12.100.

DL